ACS Biomaterials SCIENCE & ENGINEERING

Article

pubs.acs.org/journal/abseba

Liquid-like Solids Support Cells in 3D

Tapomoy Bhattacharjee,[†] Carmen J. Gil,[‡] Samantha L. Marshall,[†] Juan M. Urueña,[†] Christopher S. O'Bryan,[†] Matt Carstens,[§] Benjamin Keselowsky,[§] Glyn D. Palmer,[∥] Steve Ghivizzani,[∥] C. Parker Gibbs,[∥] W. Gregory Sawyer,[†,⊥] and Thomas E. Angelini*[,†,§]

[†]Department of Mechanical & Aerospace Engineering, 571 Gale Lemerand Drive, University of Florida, Gainesville, Florida 32611, United States

[‡]Department of Chemical Engineering, University of Florida, 1030 Center Drive, Gainesville, Florida 32611, United States

[§]J. Crayton Pruitt Family Department of Biomedical Engineering, 1275 Center Drive, University of Florida, Gainesville, Florida 32611, United States

[∥]Department of Orthopaedics and Rehabilitation, University of Florida, 3450 Hull Road, Gainesville, Florida 32611, United States

[⊥]Department of Material Science & Engineering, University of Florida, Gainesville, Florida 32611, United States

Supporting Information

ABSTRACT: The demands of tissue engineering have driven a tremendous amount of research effort in 3D tissue culture technology and, more recently, in 3D printing. The need to use 3D tissue culture techniques more broadly in all of cell biology is well-recognized, but the transition to 3D has been impeded by the convenience, effectiveness, and ubiquity of 2D culture materials, assays, and protocols, as well as the lack of 3D counterparts of these tools. Interestingly, progress and discoveries in 3D bioprinting research may provide the technical support needed to grow the practice of 3D culture. Here we investigate an integrated approach for 3D printing multicellular structures while using the same platform for 3D cell culture, experimentation, and assay development. We employ a liquid-like solid (LLS) material made from packed granular-scale microgels, which locally and temporarily fluidizes under the focused application of stress and spontaneously solidifies after the applied stress is removed. These rheological properties enable 3D printing of multicellular structures as well as the growth and expansion of cellular structures or dispersed cells. The transport properties of LLS allow molecular diffusion for the delivery of nutrients or small molecules for fluorescence-based assays. Here, we measure viability of 11 different cell types in the LLS medium, we 3D print numerous structures using several of these cell types, and we explore the transport properties in molecular time-release assays.

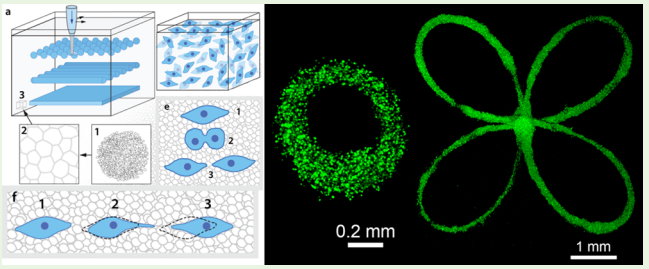

KEYWORDS: *3D printing, bioprinting, biowriting, three-dimensional cell culture, high throughput screening, tumor engineering, cancer*

INTRODUCTION

The remarkable differences between cells grown on plates and cells in vivo or in 3D culture are well-known.[1−4] At the physical level, cell shape, structure, motion, and mechanical behavior in 3D are totally different from those in the dish and are far less explored.[5−7] At the molecular level, cells grown in monolayers exhibit gene expression profiles that do not correlate or are anticorrelated with those of cells grown in 3D culture or xenograft animal models.[8−10] However, our understanding of cell biology has been heavily shaped by the culture plate, whether viewed through the lens of gene expression profiles, signaling pathways, morphological characterization, or mechanical behaviors. On the physical side of cell biology, the extensive study of migration, morphology, cytoskeletal architecture, and mechanical activity has provided a robust framework from which to describe cell behavior.[11,12] On the biomolecular side of cell biology, immunofluorescence assays combined with well-plates and plate readers have streamlined the path to characterizing cells by specific protein production levels. Closing this major gap between 2D in vitro culture and in vivo biology requires a tunable and flexible method to create 3D cell assemblies and to perform 3D cell culture in the laboratory.[13]

Jammed granular microgel particles form a liquid-like solid (LLS) material that has recently been adopted as a robust medium for the precise three-dimensional fabrication of delicate structures.[14] The microgels that constitute the LLS used here are cross-linked hydrogel particles approximately 6−7 μm in diameter. LLS materials represent an entire class of soft matter that has been exploited industrially for decades, yet has

Special Issue: 3D Bioprinting

Received: April 23, 2016
Accepted: June 1, 2016

DOI: 10.1021/acsbiomaterials.6b00218
ACS Biomater. Sci. Eng. XXXX, XXX, XXX−XXX

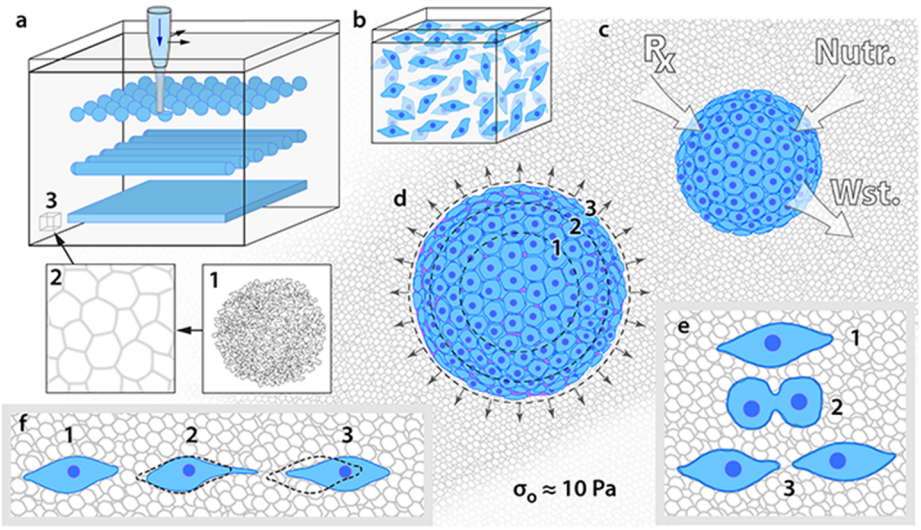

Figure 1. Liquid-like solids (LLS) as 3D culture media. (a) Low concentration microgels are packed to form liquid-like solids. The microgels used here are (a1) granular-scale (6−7 μm diameter), cross-linked hydrogel particles that form (a2) a jammed solid at high packing density. (a3) At the macroscale, the jammed microgels form a homogeneous continuum permeated with cell growth media (>99% by volume) that yields at very low applied stress. This 3D culture medium enables (a) cell assemblies to be created or (b) isolated cells to be dispersed without significant limitations. (c) Microgels' large mesh-size makes this medium highly permeable to nutrients, waste, and molecular reagents such as drugs, dyes, and proteins. (d: 1, 2, 3) Very low level of elastic stress resists the expansion of cell assemblies over time. (e, f) This expansion may be driven by cell proliferation or cell migration−processes that single cells can perform in liquid-like solids as well.

been explored by very few researchers as a 3D cell growth medium,[15−17] and has not previously been tested as a combined 3D bioprinting and culture medium. LLS materials are composed predominantly of solvent that freely diffuses and can occupy more than 99% of their volume, but they also have a finite modulus and extremely low yield stress in their solid state.[18−21] Upon yielding, LLS materials shear and behave like classical fluids; when applied stress falls below the yield stress, the LLS elastic properties recover completely.[22] This unique combination of transport, elastic, and yielding properties can be leveraged to design a support material for the maintenance of living cells in three-dimensional culture (Figure 1). Unperturbed, LLS can provide support and stability to cells and cell-assemblies. The unrestricted diffusion of nutrients, small molecules, and proteins can support the metabolic needs of cells and allows the delivery and collection of molecules. Tunable yield stress facilitates the fabrication and maintenance of precise multicellular structures, and can also provide a surmountable physical barrier that permits the migration, growth, and expansion of individual cells and cell assemblies while preventing the long-term buildup of mechanical stress.

Here we investigate the behavior of cells printed and grown in LLS 3D culture medium, quantifying cell motion and proliferation, spheroid expansion, and molecular transport both in dispersed cell populations and in printed cell-assemblies. The gentle yielding and rapid solidification behavior of this culture medium allows the unrestricted placement and structuring of cells and cell-assemblies deep within the medium. The ability of LLS to gracefully and repeatedly transition between fluidized and solid states also facilitates the precisely controlled harvesting of cell groups from targeted locations for assaying. The use of LLS in cell culture will enable new high-throughput methods for drug testing, genomic profiling, cancer screening, and personalized treatment regimens to be developed with existing infrastructure and without expensive or cumbersome instrumentation.[23]

EXPERIMENTAL SECTION

Liquid-like Solid Growth Medium Preparation. To prepare the LLS medium, we dispersed 0.9% (w/v) Carbopol ETD 2020 polymer (Lubrizol Co.) in cell growth media under sterile conditions. NaOH is added to the medium to adjust the pH to 7.4 under the incubation condition of 37 °C and 5% CO_2. The completely formulated material is homogenized in a high-speed centrifugal mixer. Carbopol ETD 2020 swells maximally at this pH, making it suitable for 3D printing and cell culture applications. The gel medium is incubated at 37 °C and 5% CO2 before printing.

Cell Culture and 3D Printing Preparation. MCF10A epithelial cells are cultured in mammary epithelial growth medium (Lonza). HUH-7 hepatocytes, A375 melanoma, PC3 prostate adenocarcinoma, MCF7 breast adenocarcinoma, MDCK and MS1 cells are cultured in high-glucose Dulbecco's modified Eagle's medium (DMEM) supplemented with 10% fetal bovine serum and 1% penicillin-streptomycin. Mesenchymal stem cells (MSC) are cultured in low-glucose Dulbecco's modified Eagle's medium (DMEM). Osteosarcoma cells (OS-156) are collected from a donor and grown in high-glucose DMEM−F12 supplemented with 10% fetal bovine serum and 1% penicillin-streptomycin. CTLL-2 cytotoxic T cells are cultured in RPMI-1640 Medium supplemented with 2 mM L-glutamine, 1 mM sodium pyruvate 10% T-STIM with Con A, 10% fetal bovine serum, and 1% penicillin-streptomycin. To 3D print cells, a concentrated cell pellet is gently sheared and loaded into a syringe. Many cell types form clusters within the syringe during 3D printing. To prevent this aggregation and achieve precise structures, we mixed hyaluronidase into the cell pellet at a final concentration of 2 mg/mL before loading into a syringe. Injection tips with an inner diameter of 100 μm are made out of glass microcapillaries (1 mm inner diameter) using a pipet puller (David Kopf Instruments) and coated with 1% pluronic F-127 solution prior to use. The 3D printing system combines a syringe pump stage (M-403.2DG from Physik Instrumente) for injecting material into the liquid-like solid medium with three linear translation stages (ILS-200PP and ILS-300PP, Newport Corporation) that provide relative motion to the injection tip. Analytical 3D functions are used to create 3D trajectories of the structures. The tangential speed of the injection tip is kept constant throughout the printing process

DOI: 10.1021/acsbiomaterials.6b00218
ACS Biomater. Sci. Eng. XXXX, XXX, XXX−XXX

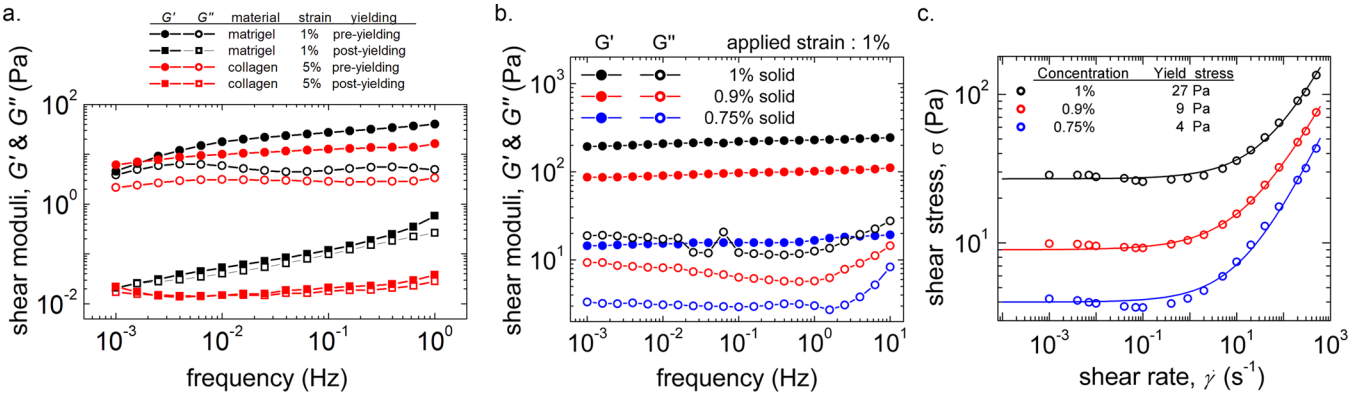

Figure 2. Rheological characterization. (a) Elastic and viscous moduli of collagen and matrigel networks show weak frequency dependence and are separated over a wide frequency range, behaving like elastic solids. However, upon yielding, these materials are permanently damaged and exhibit the rheological behaviors of viscous liquids. (b) Elastic and viscous moduli of nonyielded LLS media are flat and separated over a wide range of frequency, behaving like a Kelvin−Voigt linear solid with damping. In contrast to cross-linked polymer networks, these material properties do not change between cycles of yielding and resolidification. (c) LLS yield stress is measured by performing a strain rate sweep in which the stress is measured at many constant strain rates. Yield stress can be determined by fitting these data to a classic Herschel-Bulkley model ($\sigma = \sigma_y + k\dot{\gamma}$).

Time-Release Films for Molecular Diffusion Studies. Spherical structures of HuH-7 cells are created inside the LLS medium. To fluorescently load dyes into a time-release polymer film, we first washed ethylene-vinyl acetate (Sigma-Aldrich; 40% vinyl acetate by weight) to remove butylhydroxytoluene (BHT). A sterile 5% solution of EVA is prepared in dichloromethane. Fifty milligrams of dye containing 5 μL of DMSO is dissolved in 300 μL of EVA solution. One hundred microliters of this solution is vacuum-dried on a glass slide to create a polymer film. These time-release polymer films are placed inside the LLS medium containing HuH7 spheres. Once in the cytosol of HuH7 cells, the fluorescent dyes are activated by the cellular metabolism through the cleavage of acetoxymethyl ester groups. Celltracker green CMFDA becomes fluorescent and membrane impermeable through this process; calcein red-orange AM is intrinsically fluorescent but becomes membrane impermeable through this process so accumulates within cells over time, generating a large fluorescence signal relative to background. The spheres are imaged at different times using a confocal microscope. The local number of dye molecules per unit volume is roughly proportional to the square-root of the fluorescence intensity measured within in a confocal voxel. This signal is averaged over each sphere within the array and plotted against the distance between the polymer film and each sphere divided by the square root of time, $r/\sqrt{t}$. These data overlay onto the solution to Fick's law for the given boundary condition, $s(r, t) = s_0\left(1 - \mathrm{erf}\left(\frac{r}{2\sqrt{Dt}}\right)\right)$, using the approximate diffusion coefficients of the two dyes, D.

Fluorescence-Based Assays. Fluorescence based assays are used for 3D tracking, viability, and proliferation of cells. Cells are fluorescently dyed by treating with 10 μM 5-chloromethylfluorescein diacetate (CMFDA) in serum-free medium and 0.2% dimethyl sulfoxide for 30 min. To track MCF-10A cells in 3D, we dispersed fluorescently labeled cells into LLS growth medium at different concentrations. For identifying viability, we dispersed and incubated different types of cells in this medium and measured after the 3 and 24 h time points. Cells in LLS are stained with ReadyProbes Cell Viability Imaging Kit (Blue/Green) 15 min prior to imaging. The number of total cells (blue) and dead cells (green) are counted from the images to get viability. To study the proliferation rate of MCF-10A cells, we dyed cells with 5 μM carboxyfluorescein succinimidyl ester (CFSE) and 3D printed as spheroids within the LLS medium. The fluorescence intensity of these cells were measured over time by harvesting spheroids, dispersing the cells in liquid buffer, and performing flow cytometry, where the average decrease in fluorescence signal is inversely proportional to the number of divisions that occur between time-points.

Microscopy. Micrographs are taken with a Nikon Eclipse Ti-E microscope with a C2 confocal scanning system. Cells are imaged at 37 °C in 5% CO_2. In the case of sphere growth, cells are dyed with calcein AM before imaging. All image and video processing is done using MATLAB and ImageJ.

Cell Tracking. To explore cell−cell interactions mediated by the elasticity of the liquid-like solid medium, we create cell dispersions at many different number densities. Time-lapse 3D stacks of MCF10A cells are collected on a confocal microscope for 24 h and the cells are tracked in 3D (Figure S7 and Video 6). We characterize the average degree of cell−cell interaction by measuring the mean-square fluctuations in their length over the course of 1 h, $\langle[L(t + 1h) - L(t)]^2\rangle$ where L is the length of the longest dimension of a cell at time t, and angle brackets indicate an average over time and cell population.

RESULTS AND DISCUSSION

Cells thrive in natural 3D biopolymer networks like collagen and matrigel, as well as in engineered materials with built-in motifs for adhesion and enzymatic degradation that facilitate cell growth and migration.[24,25] The mechanical properties of these matrices prevent the precise placement or structuring of cells in 3D space, and impede continual cell culture that uses serial passaging, harvesting, and direct assaying through fluid exchange; cross-linked biopolymer networks are irreversibly damaged when yielded by the insertion of instruments and entangled polymer networks flow over long time-scales (Figure 2a). By contrast, LLS made from packed microgel particles swollen with liquid cell growth medium are nearly ideally suited for these tasks (Figure 1a, b); this material can be prepared from >99% (w/w) liquid growth media and can be poured into a container where it spontaneously flows then solidifies in one second.[14] These soft granular microgels are made from lightly cross-linked poly(acrylic acid) copolymers with a mesh size of approximately 100 nm, which allows for the nearly unimpeded diffusion of nutrients, waste, and small molecules (Figure 1c), but suppresses convective currents and thereby ensures that all molecular transport is diffusive. A low polymer concentration and correspondingly large mesh-size gives this LLS formulation a yield stress of about 10 Pa, which in turn sets an upper limit on the distortion stress that cells and cell assemblies experience (Figure 1d and Figure 2b, c). Such a low yield stress limits the buildup of pressure during cell migration and division (Figure

DOI: 10.1021/acsbiomaterials.6b00218
ACS Biomater. Sci. Eng. XXXX, XXX, XXX−XXX

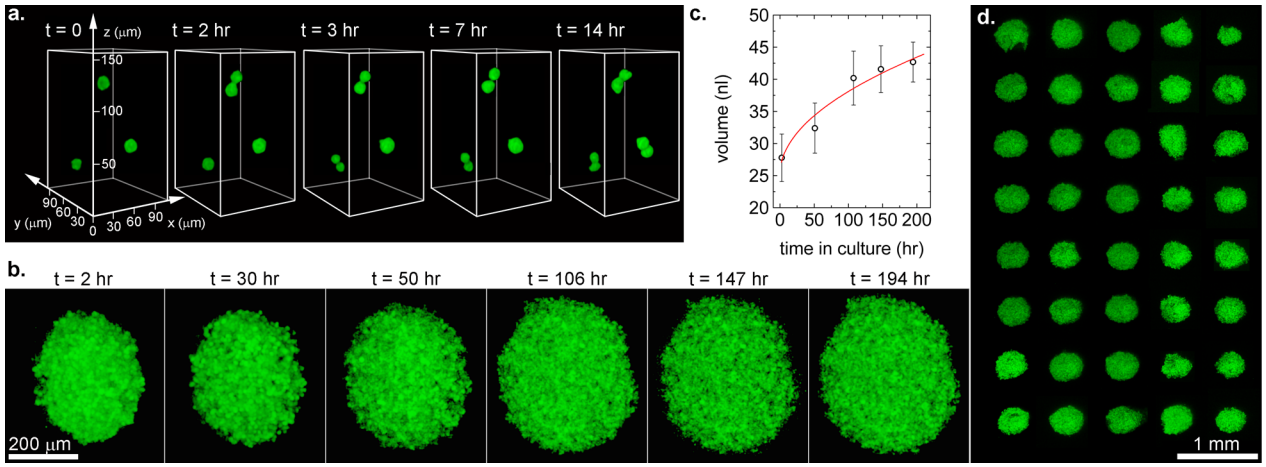

Figure 3. Cell proliferation in spheroids and in isolation. (a) MCF10A cells suspended in 3D can be seen to divide in isolation over the course of 14 h. Measurements on 1×10^4 cells reveal an average division time of 2 days. (b) Primary osteosarcoma spheroids are 3D printed into liquid-like solid growth medium and monitored with confocal microscopy (c) over the course of approximately 8 days, during which an average increase in volume of 55% is observed. Error bars are standard deviations of (d) the mean size of the 40 spheroids that were 3D printed in an array and monitored over time.

1e, f), which may be a key contributor to long duration cell viability in 3D.

The drawbacks of using natural ECM for 3D cell culture are well-recognized and have led to the development of adaptable hydrogel networks with specially designed linkages that can be reversed. Numerous different chemical and physical approaches have been developed, but the unifying concept is that the chemical equilibrium between linked and unlinked moieties kinetically controls the breaking and reforming of network junctions under localized stresses or other stimuli.[26] This principle reveals a fundamental difference between LLS and adaptable hydrogels: granular microgels are not thermal-scale objects and the jammed solid state does not arise from the kinetics of a dynamic equilibrium. Consequently, the low-strain frequency dependent rheology of the LLS does not exhibit a viscous crossover at low frequencies, corresponding to time scales as long as 10^4 s.[14] By contrast, gels with dynamic bonds exhibit fluid like rheology at low frequencies.[27] Thus, we use the term liquid-like solid to separate jammed granular microgels from other viscoelastic systems. 3D printing of hydrogels and cells into such adaptable networks has been demonstrated,[27] though in-depth research on the differences in performance between LLS and adaptable hydrogels for 3D culture and 3D printing applications has not been performed. One advantage of leveraging the jamming transition to provide the rheological properties needed for 3D printing and cell culture is that specially designed chemistries are not needed, and LLS medium can be made from a wide range of commercially available materials, facilitating its immediate use for the broader research world.

We study cell behavior in the LLS growth medium by expanding cells on standard plastic tissue culture surfaces, harvesting the cells, and either manually mixing cell dispersions or 3D printing cell structures into the LLS culture medium. We first tested the biocompatibility of microgels for live-cell culture which we have found to be noncytotoxic to 11 different cell types. Relative to cells harvested from the 2D culture dish, we have found an average viability of about 94% after 24 h in LLS culture for MDCK and MCF10A epithelial cells, MS1 and HAEC endothelial cells, HuH-7 hepatocytes, CTLL-2 killer T-cells, mesenchymal stem cells, A375 human malignant melanoma, MCF7 human breast adenocarcinoma, PC3 Caucasian prostate adenocarcinoma, and a primary osteosarcoma (Figure S1). 3D printed cocultures of HuH-7 hepatocytes and MS1 endothelial cells mixed with extracellular matrix precursor showed calcein staining for 2 weeks and exhibited physical integrity when manually transferred between culture dishes (Figure S2a). We have also serially passaged clusters of MCF10A cells into containers of fresh LLS growth media (Figure S2b).

The mechanical properties of LLS growth media enable cell division to occur with negligible physical resistance. We observe single cells dividing, during which pairs of daughter cells move apart at approximately 15 μm/h, which is comparable to the rate of cell separation in 2D culture (Figure 3a, Video 1). We estimate a strain rate within the sheared LLS granular gel during this step in cell division from the ratio of the separation speed, v, and the cell size, R, given by $\dot{\gamma} \cong v/R$, which peaks at about 1×10^{-4} s^{-1} (Figure S3). Our rheological tests of the LLS show that the stress in the medium at this strain rate is the yield stress, approximately 10 Pa (Figure 2). The cytoskeletal forces that control cell division are capable of generating much higher levels of stress than this, showing that the LLS provides cradling support in 3D but does not physically impede cell division. Proliferation occurs in large numbers within spheroids, where MCF10A cells have an average division time of 48 h—about double the time found on the well plate (Figure 3b, c, Figure S4). For cells requiring attachment through integrins or a stiffer microenvironment, natural, or synthetic ECM can be mixed into the LLS medium, improving viability (Figure S1).

Quantitative cell biology in 3D environments has been limited by the scarcity of tools that can precisely and reproducibly create model microtissues such as spheroids, and by the constraints of supporting cells in 3D. Liquid-based approaches to culturing spheroids like the hanging drop method or stirring culture provide limited control over aggregate size and involve transferring harvested spheroids between different environments for characterization. Similarly, seeding cells into polymer gels produces heterogeneous populations of cell aggregates, and optimizing the degradation rate of such polymer matrices remains a formidable challenge.[28] We overcome these limitations by 3D printing cell spheroids

DOI: 10.1021/acsbiomaterials.6b00218
ACS Biomater. Sci. Eng. XXXX, XXX, XXX−XXX

directly into the LLS with a high degree of precision and reproducibility. For example, with this method we assembled primary osteosarcoma cells into 40 spheroids with an average diameter of 380 μm and a standard deviation of 4.5% (Figure 3d). The low yield stress allows the spheres to expand unimpeded over the course of 8 days, during which spheroids increase in volume by 55% (Figure 3b, c, Figure S5, Video 2). Spheroids made from MCF10A cells expand at about twice this rate (Figure S5), whereas osteosarcoma spheroids 3D printed directly into dispersed killer T-cells show a decrease in volume and cell death over 22 h (Figure S6, Video 3). This ability to create and monitor large arrays of identical 3D microtissues contributes high throughput, precision and control to the toolbox of quantitative biology.

Equipping researchers with the ability to create complex cellular structures represents an additional way for biology to become increasingly quantitative. To take the first steps beyond spheroid based assays using LLS growth medium, we 3D print a series of simple structures having features finer than the point of a pin, with feature thicknesses as small as a few cell diameters (Figure 4). Considering that such different structures can be made from the same type of cells (MCF10A in this case), an intriguing question arises about the relationship between multicellular structure and multicellular behavior. For example, MCF10A spheroids form functional gland-like structures, called acini, when cultured in 3D matrigel networks,[29] yet their in vivo counterparts are macroscale glands composed of hollow tubular networks that connect numerous acini. We envision a future in which 3D printing into LLS culture medium is used for such mesoscale morphogenesis research. Here we have demonstrated the ability to arrange cells into complex, spatially organized structures, yet in moving forward it will be essential to investigate the integration of cells into continuously interconnected, tissuelike structures by studying the potential formation of cell−cell adhesions or indirect connections through shared extracellular matrix.

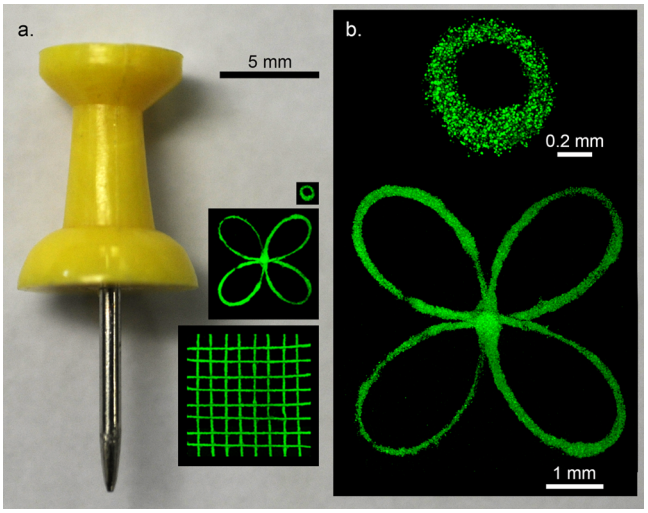

Figure 4. 3D printed fine cellular structures. (a) MCF10A cells are assembled into precise multicellular structures by 3D printing into the LLS growth medium. A cross-hash network, a four-lobed lemniscate, and a single loop are displayed to scale, relative to a push-pin. These images are maximum intensity projections of image stacks collected using confocal fluorescence microscopy. (b) Lemniscate and the single-loop micrographs are blown up to reveal feature thickness as small as a few cells in size.

The movement of tissue cells embedded in LLS is intriguing; as a cell moves, the granular gel is displaced in the direction of travel and spontaneously flows to fill the space behind the cell. This is in sharp contrast to the migration behavior in polymer networks and 3D interstitial tissue, in which 3D migration is enabled through the creation of permanent tunnels through enzymatic degradation.[30] We have observed a wide range of complex behaviors that are generally thought to require anchoring in dispersed cells without the addition of natural or synthetic extracellular matrix that possesses integrin binding domains. For example, MCF10A cells extend long filapodia that tortuously explore 3D space as if navigating through an inanimate continuum of tissue, searching for receptors of other cells. These filapodia are frequently larger than the central cell body, exceeding 30 μm in length (Figure 5a, Video 4). During

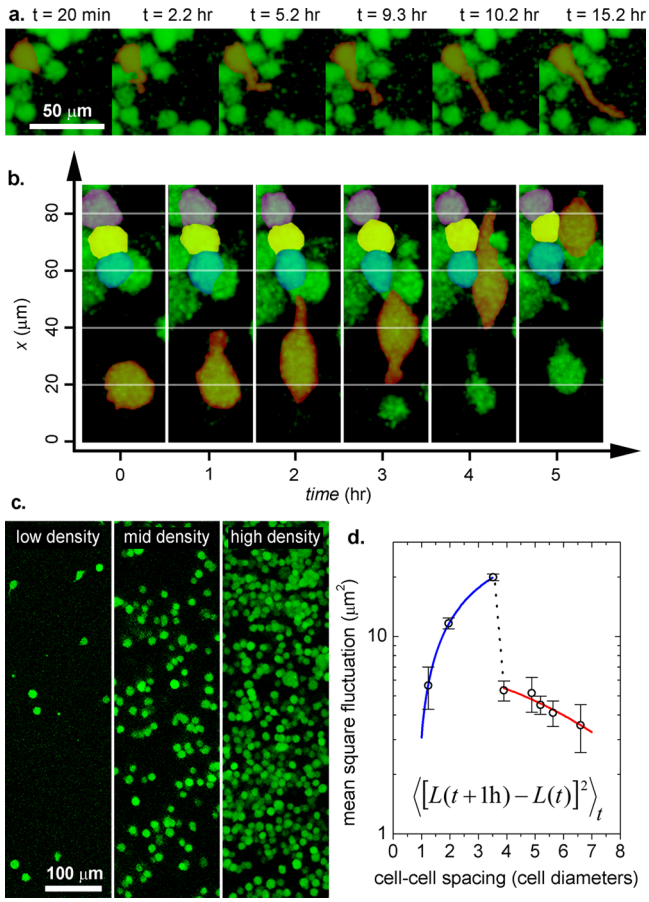

Figure 5. Cell motion in liquid-like solids. (a) MCF10A cells dispersed in liquid-like solid growth medium often extend extremely long, narrow filapodia that explore tortuous paths through the microgel particles. (b) Similar filapodia are formed during the single-cell migration process in which a cell drives a narrow protrusion through the microgel, moves the bulk of its body forward while leaving a small protrusion in its wake, and repeats the cycle to continue migrating. (c) Cells are dispersed in the liquid-like solid at different number densities which correspond to different average cell−cell spacing. (d) Cell bodies undulate with different amplitudes as a function of their spacing, indicating the role of cell−cell interactions within liquid-like solids. When cells are very sparse, their motions are very small; cells at intermediate densities fluctuate dramatically; cells packed together at high densities move very little.

DOI: 10.1021/acsbiomaterials.6b00218
ACS Biomater. Sci. Eng. XXXX, XXX, XXX−XXX

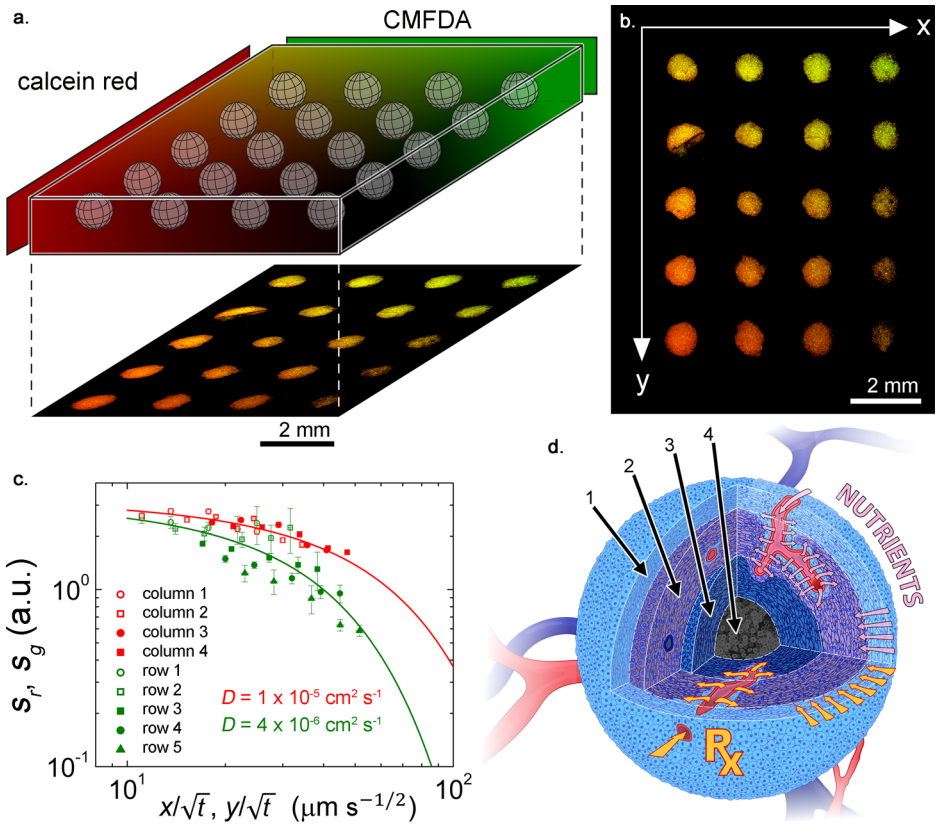

Figure 6. Transport in liquid-like solid growth medium. (a) Time-release polymer films were loaded with fluorescent dyes that are activated by cellular metabolism once in the cytosol of HUH7 hepatocytes (green hues, CMFDA; red hues, calcein red-orange AM). (b) Two-dimensional gradient of dye uptake is observed in spheroids made from HUH7 cells, where green signal is dominant in the upper right, red signal is dominant in the lower left, an intense mix of red and green is observed in the upper left, and the weakest combined signal is seen in the lower right. (c) These images can be quantitatively analyzed and plotted on a single time-space plot, showing the collapse of the red and green signals onto two predicted trend lines (red symbols, calcein red-orange AM; green symbols, CMFDA). (d) Mechanical and transport properties of the liquid-like solid growth medium, combined with 3D printing of spheroids will provide precision and control for tumor science and engineering research. The interplay between tumor volume and mass transport can be manipulated to study spatial heterogeneity in malignancy, chemotherapy resistance, proliferation rate, and necrosis (1, 2, 3, 4), and to develop effective personalized therapies by screening 3D printed spheroids made from patients' cells.

migration, we observe cells cyclically extending directed protrusions, then propelling their bodies forward in the same direction, leaving a trailing protrusion that finally retracts forward (Figure 5b, Video 5). In LLS with a yield stress of 10 Pa, the migration that proceeds by repeating this cycle requires the generation of protrusion forces on the order of 1 pN distributed across the cell surface at a spacing of about 300 nm, which fall within the range of actin polymerization forces and cytoskeletal mesh size.[31]

Precise measurement and quantitative analysis of cell-generated stress and strain in 3D environments are needed to deepen our understanding of cell mechanics within tissues, which is severely impaired by the heterogeneous microstructure of biopolymer networks. By contrast, the LLS culture medium provides a homogeneous continuum for investigating 3D problems in cell mechanics, such as cell−cell interactions mediated by a 3D continuum. We explore cell−cell interactions by dispersing MCF10A cells in the LLS medium at different number-densities, tracking the cells in 3D over time, and measuring the root-mean-square fluctuations in their length (Figure 5 c, d, Figure S7, Video 6). We find a nonmonotonic trend in this measure of cell activity as a function of cell density. At the lowest cell densities where the cells are far apart, activity is low; RMS length fluctuations are on the order of 2 μm. The fluctuations are also low at the highest densities, where the cells approach close packing and begin to cluster. This suppression of motion at high-packing densities is consistent with the behavior of cells in densely packed 3D printed spheroids, where cells are not observed to disperse from the large cell aggregates.

Cell activity is maximal and greatly amplified at intermediate cell densities; at an average center-to-center cell spacing of approximately three cell diameters the cells fluctuate in length by about 40% on average (Video 7). The detailed mechanism underlying this cell−cell stimulation could be chemical or mechanical; the concentration of excreted chemokine will decay sharply in 3D, as will strain fields generated by cell motion. We have observed an intriguing potential mechanism of cell−cell interaction by embedding fluorescent microspheres in the LLS and imaging the volumes around embedded fluorescent cells: a thick exclusion zone around the cell body, separating the cell from the LLS by about one cell diameter (Figure S8). We observe this exclusion zone immediately after dispersing the cells, so we speculate that it is filled with a pericellular matrix that many cell types produce in great abundance.[32] Moreover, when 3D printing these cells, we must add hyaluronidase to the cell growth medium to prevent cell aggregation within the injection syringe; hyaluronidase cleaves the hyaluronan component of the pericellular matrix. By contrast, we have only observed this exclusion corona when dispersing cells manually to study their individual behavior, where no

DOI: 10.1021/acsbiomaterials.6b00218
ACS Biomater. Sci. Eng. XXXX, XXX, XXX−XXX

hyaluronidase is used. In future work, quantitative studies of the diverse cell−cell interactions will be facilitated by the extremely homogeneous transport and mechanical properties of liquid-like solids.

Screening for the cooperative effects of multiple bioactive agents in combination requires large numbers of tests that are typically performed serially. To accelerate combinatorial testing on 3D cell assemblies, we can create spatiotemporal concentration gradients of multiple molecular species with quantitative control inside of the LLS. Thus, quantitative predictions of molecular concentration profiles within the LLS are possible if boundary conditions are known. To test this potential use of LLS growth medium, we embed controlled-release polymer films within the LLS to create two perpendicular boundaries that maintain a constant concentration of diffusing species. The films release dyes that contain acetoxymethyl ester groups that are enzymatically degraded by living cells once absorbed. This metabolic process activates the fluorescence of CMFDA dye and causes calcein red-orange dye to become membrane impermeable and accumulate in cells over time. Dye uptake is monitored in time-lapse confocal fluorescence imaging of 3D printed arrays of HUH7 hepatocyte spheroids (Video 8). We find that the integrated fluorescence signals from the two dye species in each sphere collapse onto two universal space-time scaling curves with no free parameters. A simple Fickian diffusion model with fixed boundary concentrations predicts the scaling of all data using molecular diffusion coefficients estimated from the published literature (Figure 6a−c, Methods). This laboratory demonstration paves the way for high-throughput combinatorial screening methods that extend further into 3D; with one printing nozzle we have generated a 3D array of 1000 spheres in less than 1 h (Figure 7).

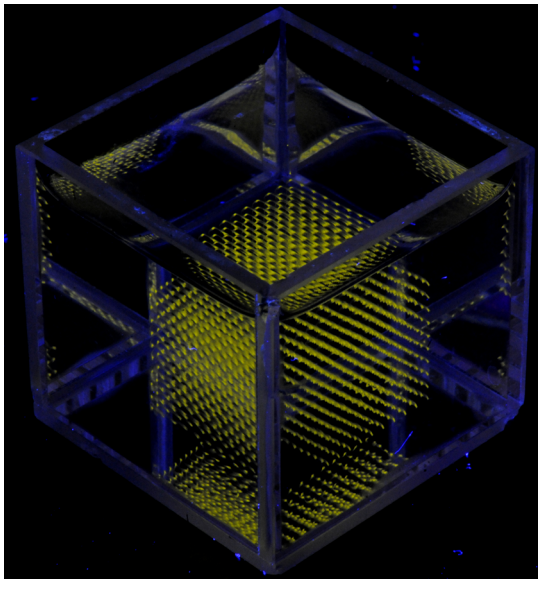

Figure 7. 3D printed array of spheres. Precision 3D printing in the LLS medium enables the high speed manufacture of small simple structures like spheres. Here, an array of 1000 spheres made from fluorescent colloids is shown within a 2 in. quartz cube. This 3D approach may be extended to cell spheroid culture, where high-throughput screening for drug discovery and personalized therapies can be envisioned.

CONCLUSION

The need is clear for screening and analysis methods using 3D cell culture. In addition to changes in cell architecture and cell−cell interactions, 3D assemblies of cells in vivo and in vitro possess an inside−outside asymmetry and accompanying chemical and mechanical gradients that are tied to the very foundations of tissue complexity; these gradients do not exist in 2D (Figure 6d). To this end, the use of LLS as a 3D culture medium allows the tools of 2D molecular and cell biology to be repurposed for 3D without technical barriers. Much like tissue culture plastic, the LLS growth media does not itself replicate a physiological environment. Instead, its extremely high levels of tunability and versatility allow the cellular environment to be manipulated with minimal restrictions. In the absence of large applied stresses, the LLS is stable under the gravitational forces on embedded cellular structures. We estimate an approximate limit to the size of a spherical structure that could be supported by the LLS through a simple force balance. For a tissue spheroid of radius R having a mass density of muscle (about 6% higher than water), the gravitational downward force is given by $\frac{4}{3}\pi R^3 \Delta\rho g$, where g is the acceleration due to gravity and $\Delta\rho$ is the density mismatch between the tissue and the LLS. This force must be balanced by the LLS for stability, which is approximately given by $\pi R^2 \sigma_y$, where σ_y is the LLS yield stress. This force balance predicts that a dense sphere of muscle-like tissue will sink in the LLS if its diameter exceeds about 2.5 cm, or one inch. Our observations are consistent with this prediction; we have not observed 3D printed spheroids sinking during time-lapse imaging.

The reversible fluid−solid transition of LLS facilitates the tasks of 2D culture such as seeding, feeding, and passaging to be performed by hand or in well-plates with high-throughput robotic pipetting and incubation systems, as well as fluorescence or luminescence assaying with plate-readers. Cells can be 3D printed into arbitrarily complex structures or randomly dispersed directly into well plates or any culture vessel. Transport and material properties can be tuned by varying the polymer concentration in the LLS. Imaging can be performed directly in the LLS or cells and cell assemblies at targeted locations can be harvested for analysis without disturbing surrounding material. An unbounded multitude of applications of LLS 3D culture can be envisioned, from screening for personalized cancer treatments to tissue engineering, to fundamental cell biology.

ASSOCIATED CONTENT

Supporting Information

The Supporting Information is available free of charge on the ACS Publications website at DOI: 10.1021/acsbiomaterials.6b00218.

Detailed information about cell division, proliferation ,and viability in LLS; 3D printed array of spheres and spheroid growth; coculture of cytotoxic T-cells and 3D printed osteosarcoma tumor; Figures S1−S8 (PDF)

Supporting Video 1, cell division in 3D: Reconstruction of a time lapse confocal z-stack showing three MCF 10A cells dividing within the LLS culture medium (AVI)

Supporting Video 2, spheroid growth in LLS growth medium: time-lapse of 40 osteosarcoma spheroids over a course of 9 days imaged with confocal fluorescence microscopy (AVI)

DOI: 10.1021/acsbiomaterials.6b00218
ACS Biomater. Sci. Eng. XXXX, XXX, XXX−XXX

Supporting Video 3, coculture of cytotoxic T-cells and an osteosarcoma tumor in 3D: time-lapse images show the migration of cytotoxic T-cells (CTLL-2) in 3D; osteosarcoma tumor (red) shrinks in the LLS medium when cultured in the presence of killer T-cells (green) (AVI)

Supporting Video 4, cell extending filapodium in 3D: 3D time lapse from reconstructed confocal imaging shows MCF 10A cells extending filapodia in 3D (AVI)

Supporting Video 5, cell migration in 3D: time lapse of a 3D reconstructed confocal image of MCF 10A cells migrating in 3D through the LLS growth medium (AVI)

Supporting Video 6, cell tracking in 3D: reconstruction from a time lapse confocal imaging of three MCF 10A cells embedded in LLS growth medium (green) with their tracked centroids (red) overlaid (AVI)

Supporting Video 7, cell−cell interactions in 3D. Maximum intensity z-projection time lapse of MCF 10A cells interacting in 3D through the LLS growth medium (AVI)

Supporting Video 8, molecular transport through LLS growth medium; maximum intensity z-projection time lapse of confocal images shows the uptake of dyes by a grid of HuH-7 hepatocyte spheroids (AVI)

AUTHOR INFORMATION

Corresponding Author

*E-mail: t.e.angelini@ufl.edu.

Author Contributions

The manuscript was written through contributions of all authors. All authors have given approval to the final version of the manuscript.

Funding

This work was funded by the National Science Foundation under Grant DMR-1352043 and by Lubrizol Life Sciences.

Notes

The authors declare no competing financial interest.

REFERENCES

(1) Baker, B. M.; Chen, C. S. Deconstructing the third dimension−how 3D culture microenvironments alter cellular cues. *J. Cell Sci.* **2012**, *125* (13), 3015−3024.

(2) Fraley, S. I.; Feng, Y.; Krishnamurthy, R.; Kim, D.-H.; Celedon, A.; Longmore, G. D.; Wirtz, D. A distinctive role for focal adhesion proteins in three-dimensional cell motility. *Nat. Cell Biol.* **2010**, *12* (6), 598−604.

(3) Cukierman, E.; Pankov, R.; Stevens, D. R.; Yamada, K. M. Taking cell-matrix adhesions to the third dimension. *Science* **2001**, *294* (5547), 1708−1712.

(4) Hutmacher, D. W. Biomaterials offer cancer research the third dimension. *Nat. Mater.* **2010**, *9* (2), 90−93.

(5) Herrmann, D.; Conway, J. R.; Vennin, C.; Magenau, A.; Hughes, W. E.; Morton, J. P.; Timpson, P. Three-dimensional cancer models mimic cell−matrix interactions in the tumour microenvironment. *Carcinogenesis* **2014**, *35* (8), 1671−1679.

(6) Wirtz, D.; Konstantopoulos, K.; Searson, P. C. The physics of cancer: the role of physical interactions and mechanical forces in metastasis. *Nat. Rev. Cancer* **2011**, *11* (7), 512−522.

(7) Doyle, A. D.; Wang, F. W.; Matsumoto, K.; Yamada, K. M. One-dimensional topography underlies three-dimensional fibrillar cell migration. *J. Cell Biol.* **2009**, *184* (4), 481−490.

(8) Sieh, S.; Taubenberger, A. V.; Rizzi, S. C.; Sadowski, M.; Lehman, M. L.; Rockstroh, A.; An, J.; Clements, J. A.; Nelson, C. C.; Hutmacher, D. W. Phenotypic characterization of prostate cancer LNCaP cells cultured within a bioengineered microenvironment. *PLoS One* **2012**, *7* (9), e40217.

(9) Luca, A. C.; Mersch, S.; Deenen, R.; Schmidt, S.; Messner, I.; Schäfer, K.-L.; Baldus, S. E.; Huckenbeck, W.; Piekorz, R. P.; Knoefel, W. T.; et al. Impact of the 3D microenvironment on phenotype, gene expression, and EGFR inhibition of colorectal cancer cell lines. *PLoS One* **2013**, *8* (3), e59689.

(10) Gibbs, C. P.; Kukekov, V. G.; Reith, J. D.; Tchigrinova, O.; Suslov, O. N.; Scott, E. W.; Ghivizzani, S. C.; Ignatova, T. N.; Steindler, D. A. Stem-like cells in bone sarcomas: implications for tumorigenesis. *Neoplasia* **2005**, *7* (11), 967−976.

(11) Fletcher, D. A.; Mullins, R. D. Cell mechanics and the cytoskeleton. *Nature* **2010**, *463* (7280), 485−492.

(12) Discher, D. E.; Janmey, P.; Wang, Y.-l. Tissue cells feel and respond to the stiffness of their substrate. *Science* **2005**, *310* (5751), 1139−1143.

(13) Pampaloni, F.; Reynaud, E. G.; Stelzer, E. H. The third dimension bridges the gap between cell culture and live tissue. *Nat. Rev. Mol. Cell Biol.* **2007**, *8* (10), 839−845.

(14) Bhattacharjee, T.; Zehnder, S. M.; Rowe, K. G.; Jain, S.; Nixon, R. M.; Sawyer, W. G.; Angelini, T. E. Writing in the granular gel medium. *Science advances* **2015**, *1* (8), e1500655.

(15) Ravindran, S.; Roam, J. L.; Nguyen, P. K.; Hering, T. M.; Elbert, D. L.; McAlinden, A. Changes of chondrocyte expression profiles in human MSC aggregates in the presence of PEG microspheres and TGF-β3. *Biomaterials* **2011**, *32* (33), 8436−8445.

(16) Nguyen, P. K.; Snyder, C. G.; Shields, J. D.; Smith, A. W.; Elbert, D. L. Clickable Poly (ethylene glycol)-Microsphere-Based Cell Scaffolds. *Macromol. Chem. Phys.* **2013**, *214* (8), 948−956.

(17) Roam, J. L.; Yan, Y.; Nguyen, P. K.; Kinstlinger, I. S.; Leuchter, M. K.; Hunter, D. A.; Wood, M. D.; Elbert, D. L. A modular, plasmin-sensitive, clickable poly (ethylene glycol)-heparin-laminin microsphere system for establishing growth factor gradients in nerve guidance conduits. *Biomaterials* **2015**, *72*, 112−124.

(18) Dimitriou, C. J.; Ewoldt, R. H.; McKinley, G. H. Describing and prescribing the constitutive response of yield stress fluids using large amplitude oscillatory shear stress (LAOStress). *J. Rheol. (Melville, NY, U. S.)* **2013**, *57* (1), 27−70.

(19) Fernandez-Nieves, A.; Wyss, H.; Mattsson, J.; Weitz, D. A. *Microgel Suspensions: Fundamentals and Applications*; John Wiley & Sons: New York, 2010.

(20) Menut, P.; Seiffert, S.; Sprakel, J.; Weitz, D. A. Does size matter? Elasticity of compressed suspensions of colloidal-and granular-scale microgels. *Soft Matter* **2012**, *8* (1), 156−164.

(21) Mattsson, J.; Wyss, H. M.; Fernandez-Nieves, A.; Miyazaki, K.; Hu, Z.; Reichman, D. R.; Weitz, D. A. Soft colloids make strong glasses. *Nature* **2009**, *462* (7269), 83−86.

(22) Coussot, P.; Tocquer, L.; Lanos, C.; Ovarlez, G. Macroscopic vs. local rheology of yield stress fluids. *J. Non-Newtonian Fluid Mech.* **2009**, *158* (1), 85−90.

(23) Isherwood, B.; Timpson, P.; McGhee, E. J.; Anderson, K. I.; Canel, M.; Serrels, A.; Brunton, V. G.; Carragher, N. O. Live cell in vitro and in vivo imaging applications: accelerating drug discovery. *Pharmaceutics* **2011**, *3* (2), 141−170.

(24) Seliktar, D. Designing cell-compatible hydrogels for biomedical applications. *Science* **2012**, *336* (6085), 1124−1128.

(25) Tibbitt, M. W.; Anseth, K. S. Hydrogels as extracellular matrix mimics for 3D cell culture. *Biotechnol. Bioeng.* **2009**, *103* (4), 655−663.

(26) Wang, H.; Heilshorn, S. C. Adaptable hydrogel networks with reversible linkages for tissue engineering. *Adv. Mater.* **2015**, *27* (25), 3717−3736.

(27) Highley, C. B.; Rodell, C. B.; Burdick, J. A. Direct 3D Printing of Shear-Thinning Hydrogels into Self-Healing Hydrogels. *Adv. Mater.* **2015**, *27* (34), 5075−5079.

(28) Place, E. S.; Evans, N. D.; Stevens, M. M. Complexity in biomaterials for tissue engineering. *Nat. Mater.* **2009**, *8* (6), 457−470.

(29) Petersen, O. W.; Rønnov-Jessen, L.; Howlett, A. R.; Bissell, M. J. Interaction with basement membrane serves to rapidly distinguish growth and differentiation pattern of normal and malignant human

DOI: 10.1021/acsbiomaterials.6b00218
ACS Biomater. Sci. Eng. XXXX, XXX, XXX−XXX

breast epithelial cells. *Proc. Natl. Acad. Sci. U. S. A.* **1992**, *89* (19), 9064−9068.
(30) Wolf, K.; Te Lindert, M.; Krause, M.; Alexander, S.; Te Riet, J.; Willis, A. L.; Hoffman, R. M.; Figdor, C. G.; Weiss, S. J.; Friedl, P. Physical limits of cell migration: control by ECM space and nuclear deformation and tuning by proteolysis and traction force. *J. Cell Biol.* **2013**, *201* (7), 1069−1084.
(31) Howard, J. *Mechanics of Motor Proteins and the Cytoskeleton*; Sinauer Associates: Sunderland, MA, 2001.
(32) McLane, L. T.; Chang, P.; Granqvist, A.; Boehm, H.; Kramer, A.; Scrimgeour, J.; Curtis, J. E. Spatial organization and mechanical properties of the pericellular matrix on chondrocytes. *Biophys. J.* **2013**, *104* (5), 986−996.

DOI: 10.1021/acsbiomaterials.6b00218
ACS Biomater. Sci. Eng. XXXX, XXX, XXX−XXX

Supporting Information for

Liquid-like Solids Support Cells in 3D

*Tapomoy Bhattacharjee[1], Carmen J. Gil[2], Samantha L. Marshall[1], Juan M. Urueña[1], Christopher S. O'B'ryan[1], Matt Carstens[3], Benjamin Keselowsky[3], Glyn D. Palmer[4], Steve Ghivizzani[4], C. Parker Gibbs[4], W. Gregory Sawyer[1, 5], Thomas E. Angelini[1, 3]**

[1]Department of Mechanical & Aerospace Engineering, 571 Gale Lemerand Drive, University of Florida, Gainesville FL, 32611

[2]Department of Chemical Engineering, University of Florida, 1030 Center Drive, Gainesville FL, 32611

[3]J. Crayton Pruitt Family Department of Biomedical Engineering, 1275 Center Drive, University of Florida, Gainesville FL, 32611

[4]Department of Orthopaedics and Rehabilitation, University of Florida, 3450 Hull Road, Gainesville FL, 32611

[5]Department of Material Science & Engineering, University of Florida, Gainesville FL, 32611

Keywords: 3D printing; bioprinting; biowriting; three dimensional cell culture; high throughput screening; tumor engineering; cancer

Number of pages: 6

Number of figures: 8

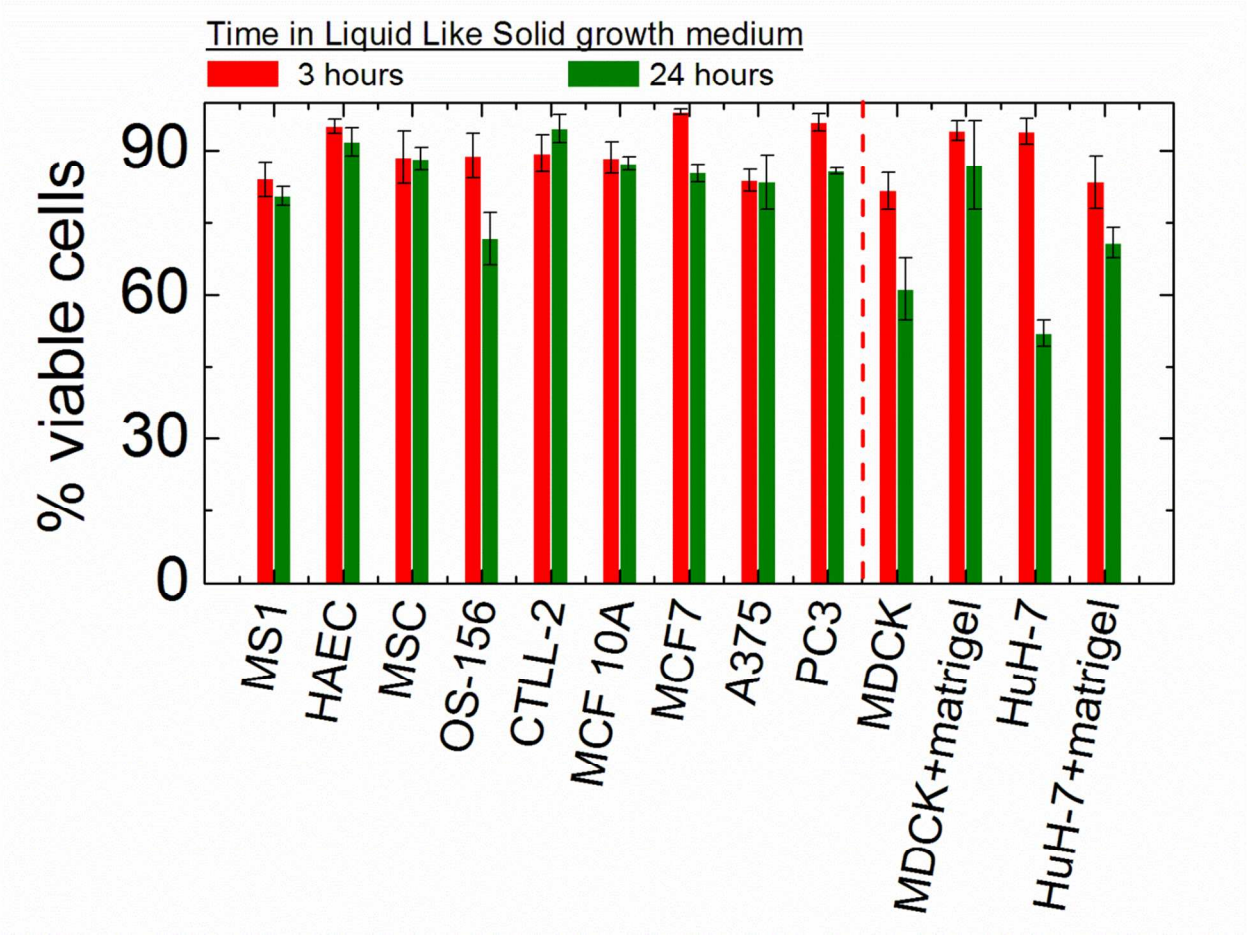

Figure S1. Cell Viability. Eleven different cell lines are dispersed and incubated in liquid like solid medium for 3 hours and 24 hours respectively to explore short term cell viability. ReadyProbes Cell Viability Imaging Kit (Life Technologies) is used to stain all the cells and dead cells. Cell counts (total & dead) obtained from confocal microscope images are used to determine the viability. Relative to cells harvested from the 2D culture dish (3 hour time-point), we have found an average viability of about 94% after 24 hours (Table 1 in main text). Endothelial cells, MS1 (MILE SVEN 1) and HAEC (Human Aortic Endothelial Cells) along with Mesenchymal Stem Cells (MSC), cytotoxic T cells (CTLL-2) and non-tumorigenic human epithelial cell line MCF10A exhibit an absolute viability of approximately 90% after incubation inside the LLS medium for 24 hours. Primary osteosarcoma cells (OS) along with other cancer cell lines such as human malignant melanoma (A375), Human Breast Adenocarcinoma (MCF7), Caucasian prostate adenocarcinoma (PC3) also show high viability in LLS medium. Interestingly, to achieve this high viability with Madin Darby Canine Kidney (MDCK) cells and human hepatoma cells (HuH-7), a supplemental matrix (matrigel) must be co-dispersed with the cells into the LLS medium.

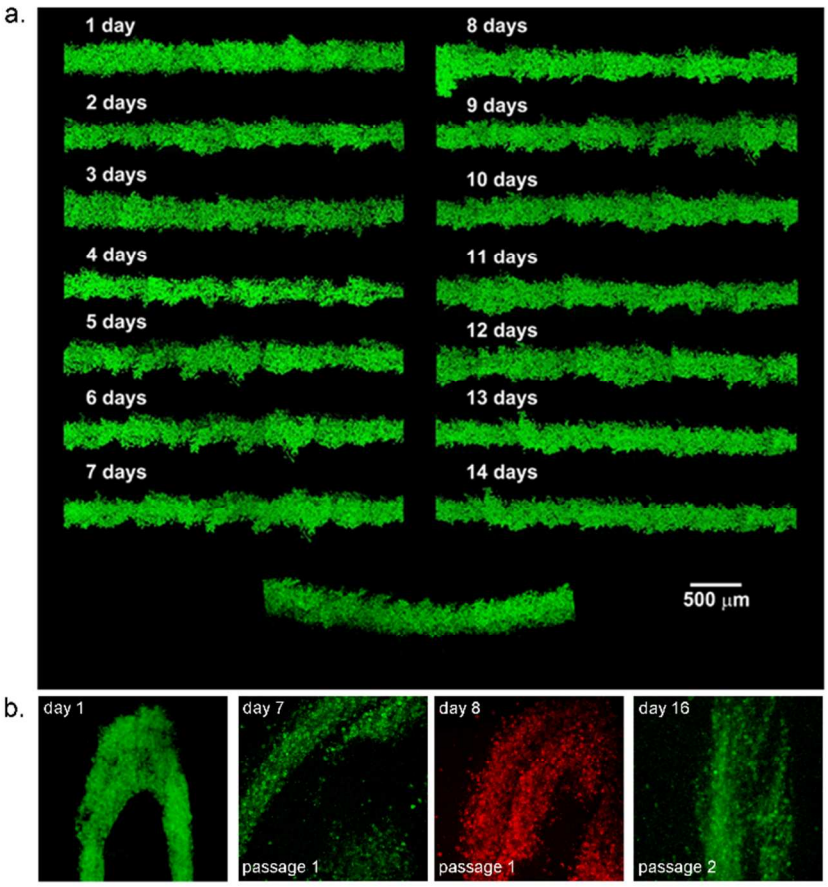

Figure S2. Passaging cells in LLS medium. (a) Cylindrical structures of HuH-7 cells were printed in liquid like solid growth media. This structure was monitored for 2 weeks before removing and imaging in liquid culture media. (b) Aggregates of MCF10A were created inside LLS growth media. The solid structure of MCF10A was dyed with calcein-AM (day 1) and incubated inside the LLS for 7 days. On day 7, this structure was removed and placed inside a fresh LLS bath (day 7, passage 1). This structure was dyed with calcein red on day 8 to confirm the continued metabolic activity of cells and observe the presence of new cells. On day 16, the structure was passaged and dyed with calcein green for a second time, where the persistence of cell viability was observed.

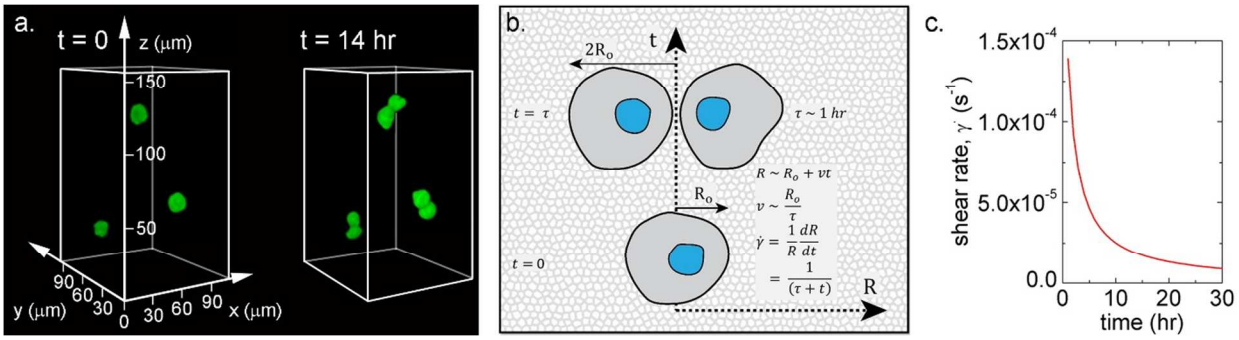

Figure S3. Yield stress and cell division. MCF10A cells can divide while supported by the liquid like solid medium (a). During division as the two daughter cells separate, they strain the surrounding medium by expanding from an initial size-scale, R_0 to a larger size-scale which we approximate to be $2R_0$. Treating this expansion to scale linearly with time, we estimate a strain-rate which depends on the time, τ, over which the daughter cells move apart (b). The maximum shear that occurs during this process is extremely low, falling in a regime where viscous stresses are negligible compared to the Herschel-Bulkley yield stress (c). Thus, isolated cells only have to generate approximately 10 Pa of stress to divide.

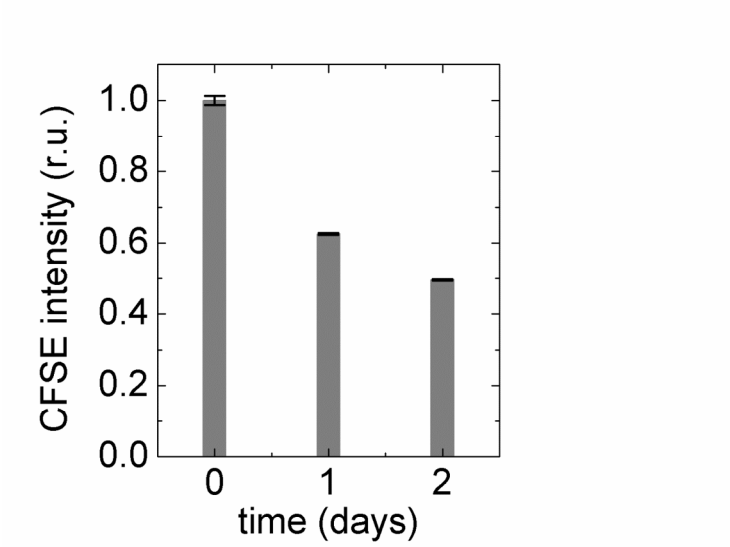

Figure S4. Proliferation. MCF10A cells were dyed with 5 μM Carboxy-fluorescein succinimidyl ester (CFSE) and spheroids are printed inside a bath of liquid like solid. Spheroids at three different time points are harvested from the liquid like solid media and dispersed. To measure proliferation, fluorescence intensities of 10^4 cells from these spheroids are measured in a flow cytometer. The fractional decrease in fluorescence intensity is the reciprocal of the number of division cycles that have occurred. Thus, this proliferation study shows a cell doubling time of two days in liquid like solid medium.

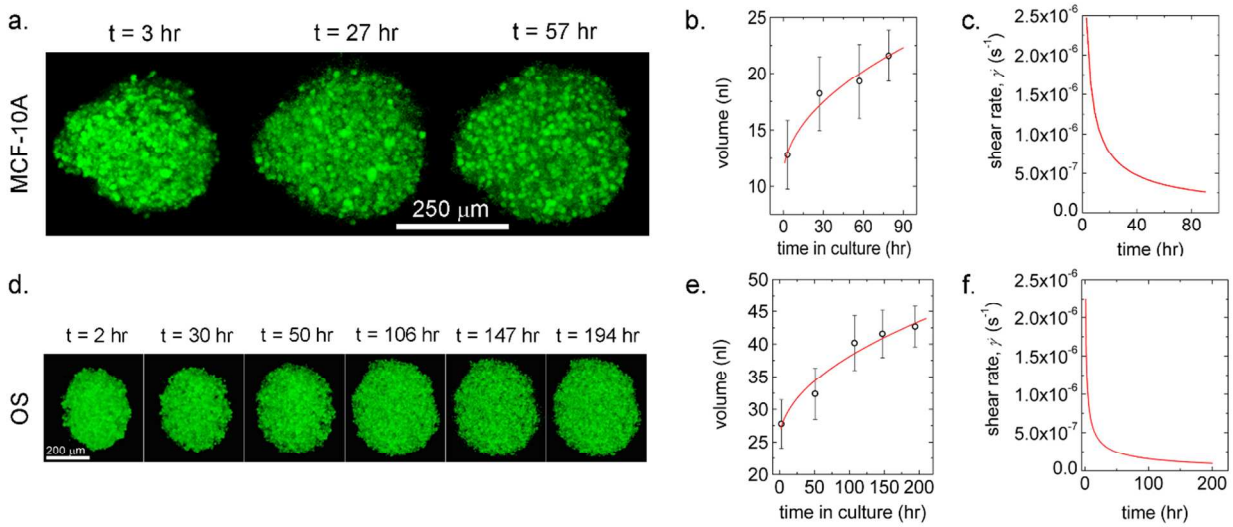

Figure S5. Spheroid growth in liquid like solid medium. MCF10A and primary osteosarcoma spheroids are created in liquid like solid medium and dyed with caldein-AM (a,d). Maximum intensity projections of confocal images are analyzed to measure the spheroid diameters and to determine spheroid volume. Spheroid volume scales approximately like the square-root of time (b,e). Shear rates of these sphere growths are calculated as $\dot{\gamma} = R^{-1} dR/dt$, where R is the spheroid radius and t is time (c,f). The shear rate associated with spheroid growth always falls in the plateau region of the LLS yielding curve which ensures that the spheroid is under a constant stress equal to the yield stress.

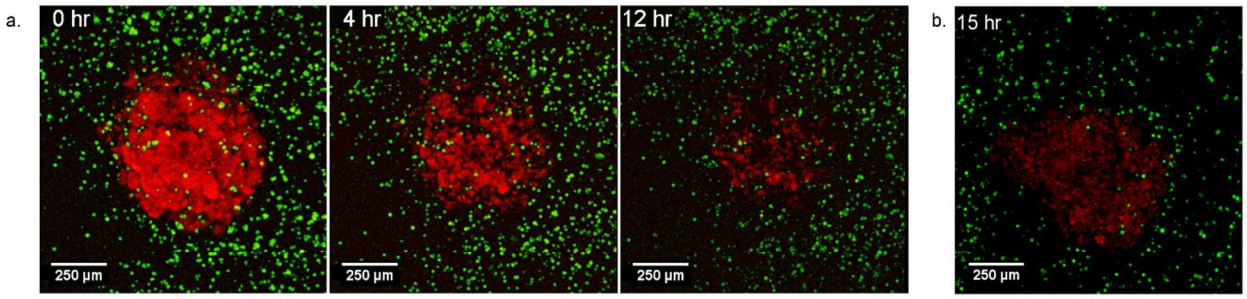

Figure S6. Co-culture of cytotoxic T-cells and 3D printed osteosarcoma tumor. (a) An osteosarcoma tumor (red) is printed in a dispersion of killer T-cells (green). The maximum intensity projection image of the system shows a shrinking tumor with decreasing fluorescence intensity from the vital dye (calcein-red). By contrast, the identical tumors are always observed to grow in the absence of the killer T-cells (ED fig. 7). (b) To check for potential artifacts from photobleaching, we imaged a second tumor that was never previously exposed to light after printing, finding again the reduced red fluorescence, confirming the death of OS cells.

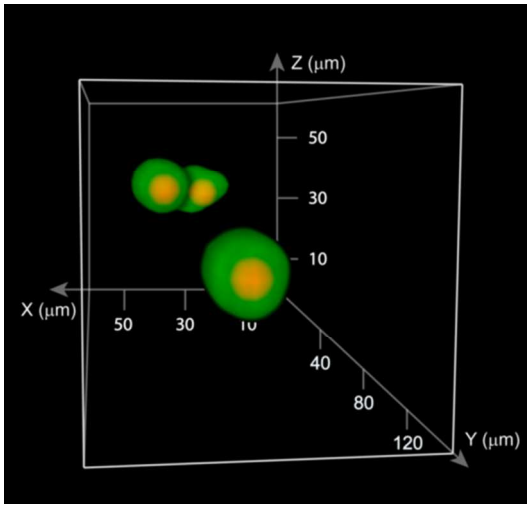

Figure S7. Three dimensional cell tracking. MCF10A cells are dyed with chloromethylfluorescein diacetate (CMFDA) and dispersed in the liquid like solid medium. A time-lapse series of 3D fluorescence images of cells are collected throughout space on an environmentally controlled confocal microscope for 20 hours (green spheres). 3D centroids of individual cells are identified and tracked over all time frames (red centers).

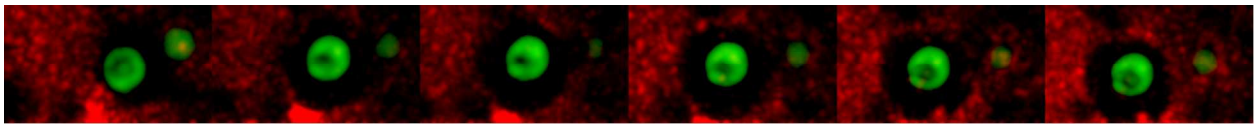

Figure S8. Pericellular matrix in 3D. MCF10A cells are dyed with CMFDA and dispersed into the LLS medium containing red fluorescent polystyrene microspheres 1 μm in diameter. The fluorescent microspheres appear to be excluded from a large zone surrounding each cell, which may be a pericellular matrix. Maximum intensity projection images show that the thickness of this excluded region is approximately one cell diameter.